Metallography, Microstructure, and Analysis (2018) 7:153–167
https://doi.org/10.1007/s13632-018-0421-x

TECHNICAL ARTICLE

A Study on the Failure of Steel Chains in Rotary Cement Kilns

M. A. M. Al-Moussawi[1,2]

Received: 25 August 2017 / Revised: 22 December 2017 / Accepted: 15 January 2018 / Published online: 30 January 2018

Abstract
The failure of steel chains which are used in rotary cement kilns costs cement companies a significant price. This study investigated the causes of chains failure at the *Kufa* cement plant and proposes new materials that can serve for a prolonged period of time. Two grades of steel chains were investigated including DIN 1.4742 (AISI 10F) and St37. Ten samples of chains from different locations from the kiln flame have been taken after 30 days and after 180 days of continuous work inside the rotary cement kiln. To study the effect of the distance from the kiln flame on the DIN 1.4742 (AISI 10F), another two samples have been replaced the St37 grade at a distance of 28.2 m. Chemical analysis for each sample under study has been carried out in order to highlight the differences between the used chain and the original chain in terms of alloying elements weight. An optical images of the unused and used chains of DIN 1.4742 (AISI 10F) steel grade have been taken to understand that the change occurs in the grain size. SEM-EDS technique was also applied to understand the possible segregation of elements. The results showed that the decrease of alloying elements pct, especially Cr, in the microstructure was the main reason of chain failure by corrosion/erosion mechanism. Preventing Cr from segregation can prolong the life of kiln chains during service. The study suggests new steel grades to replace DIN 1.4742 (AISI 10F) and St37 steel grades.

Keywords Steel chains · Cement kilns · Cr segregation

Introduction

Chains in wet and long-dry rotary cement kilns usually work as a removal of the moisture from the raw cement materials (mud), and it is also cleaning the kiln shell by transporting materials, crushing the mud rings, reducing the dust amount, and reducing the kiln exit gas temperature. Figure 1 shows a sketch to the rotary cement kiln including the chain locations (called also curtains) and the process of cement manufacturing [1]. The raw material enters the rotary cement (wet feed) with a temperature of 40 °C, while it discharges from the kiln with a temperature of 200 °C. The gas enters the kiln with a temperature usually ranged from 700 to 760 °C and exits with a temperature of 180 °C. These ranges of temperatures input and exit are controlled by the chains; any issues in the chains including failure due to breakage during the kiln operation can affect the product (clinker) quality and may result in air pollution. Figure 2 is a real image of chains curtain inside rotary cement kiln at "*Kufa cement plant*" which is under concern in this study, while Fig. 3 shows the relationship between energy consumption with and without using chain curtains [2]. The use of chains which made of carbon steel has caused in reduction in energy consumption from 1870 to 1730 kcal/kg, while using heat resistance chains cased in energy consumption of 1500 kcal/kg. Chains usually experience complicated thermo-chemical-mechanical conditions during cement kiln operation. Gas temperatures can reach to 800 °C in the first row of chains, while the temperature of raw material in contact with the chains is about 200 °C as shown in Fig. 4 [2]. Materials selection of chains usually depends on the location and the type of fuel used in cement kiln, high resistance steel grades are preferable in the first rows of chain curtains, while cheaper steel grades can be used in a distance far away from the flame to reduce the cost. Steel grades include carbon steel (AISI C1020, C1022, C1035), alloy steel (SAE 4140 and 8620), stainless ferritic steel (AISI 8F, 9F, and 10F), stainless austenitic steel (AISI 304, 329, 309, 310, and 321), and the very high resistance steel grades which have been developed by adding Mn element to increase the protection of Ni and Cr alloying elements. Figure 5 shows the ideal

✉ M. A. M. Al-Moussawi
inj.mun@atu.edu.iq; acesma4@exchange.shu.ac.uk

[1] Al-Furat Al-Awsat Technical University, Kufa, Iraq

[2] Sheffield Hallam University, Sheffield, UK

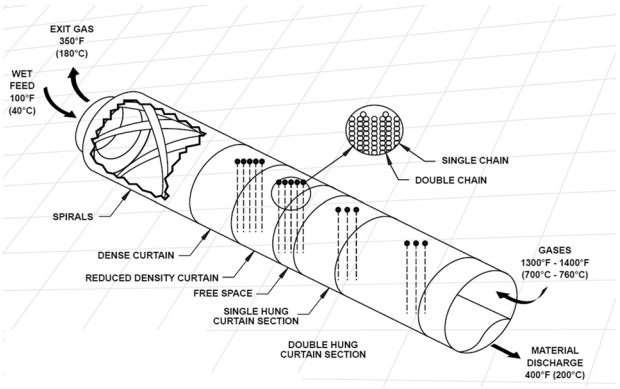

Fig. 1 A sketch to the rotary cement kiln including the chain locations (curtains) and the process of cement manufacturing [1]

Fig. 2 A real image of chains curtain inside rotary cement kiln at *Kufa cement plant*. Courtesy of *Kufa cement plant* (image no. CK-005)

suggested layout of chains designed by Heko Ketten company, Germany, which depends on the fuel type [2]. Kiln chains usually last for maximum of 10–12 months depending on the operation conditions and the type of steel grades [*Kufa cement plant* records]. Issues of corrosion, deformation, and brittleness especially in the top ring of the chain are the most causes of the chains failure. Figure 6a–e shows different types of chains failure after serving for different period of time ranging from 6 to 8 months [*Kufa cement plant*]. The failures include (a) reduction in thickness and deformation, (b) oval deformation in the top ring, (c) reduction in thickness, oval and twisting deformation in the top ring, and (d) brittle cracking.

Previous work on cement kiln chains is limited for industrial companies which produce these products such as Heko Ketten, Germany, and AMH, Canada. Corrosion and chromium segregation represent the most issues that can lead to kiln chains failure. Stavrev and Dikova [3] investigated the structural changes of cement kiln chains grade DIN 1.4892 105MA Ni, Cr, Mn steel. They found that a reduction of 30% of chains thickness has occurred after 120 days of continuous service as a result of the corrosion and the mechanical effect of the mud. The microstructure of the chains which exposed to a temperature fluctuation above 700 °C was found to experience recrystallization. This in turn has resulted in a pit character and corrosion-fatigue cracks under the cyclic mechanical load. This crack was then propagated toward the depth of the chain and caused the final failure by breakage. Park et al. 2013 [4] applied immersing of weathering steels in 16.9 vol.% H2SO4 + 0.35 vol.% HCl at 60 °C in order to investigate the effect of Cr on corrosion resistance. Cr segregation at grain boundaries was found to increase when Cu elements exist in steel. They found that microgalvanic corrosion was the mechanism of Cr segregation as the grain acts as anode, whereas the grain boundary acts as cathode. The localized segregation of Cr has been found to cause in pitting corrosion which in turn caused in a reduction in the steel thickness. Saraf et al. [5] found that Cr diffusion in Ni/Cr steels is the main issue that can reduce the corrosion resistance in steel. The Cr was found to segregate at the high-angle grain boundaries, and the angular misorientation between two grains is the driver of Cr segregation. Laws and Goodhew [6] investigated the relationship between Cr segregation and grain boundary structure of AISI 316 stainless steel using analytical electron microscopy technique (AEM). They found that the summation of boundaries which is equal to 9 was resulted in more Cr concentration rather than other grain boundaries. Defilippi and Chao [7] found that a band-like segregation pattern of chromium and molybdenum occurs in 434 stainless steel when hot rolling carried out in the temperature range of austenite and ferrite phase diagram. This type of segregation has classified as detrimental because it has led to ridging recrystallization.

The current work aims to understand the causes of kiln chains failure of *Kufa cement plant* by taking many samples of chains from different locations starting from the first row until 28.2 m. Two time periods of continuous operation have been chosen (30 and 180 days) in order to understand the progress of failure with time. Chemical analysis, optical microscopy, and SEM-EDS techniques have been employed to investigate the possible phase change, grain growth, and elemental segregation.

Materials and Methods

Kufa cement plant depends on a wet process production with 4881 chains inside the rotary cement kiln, and each chain includes 45 rings. Heavy oil has been used as a fuel during

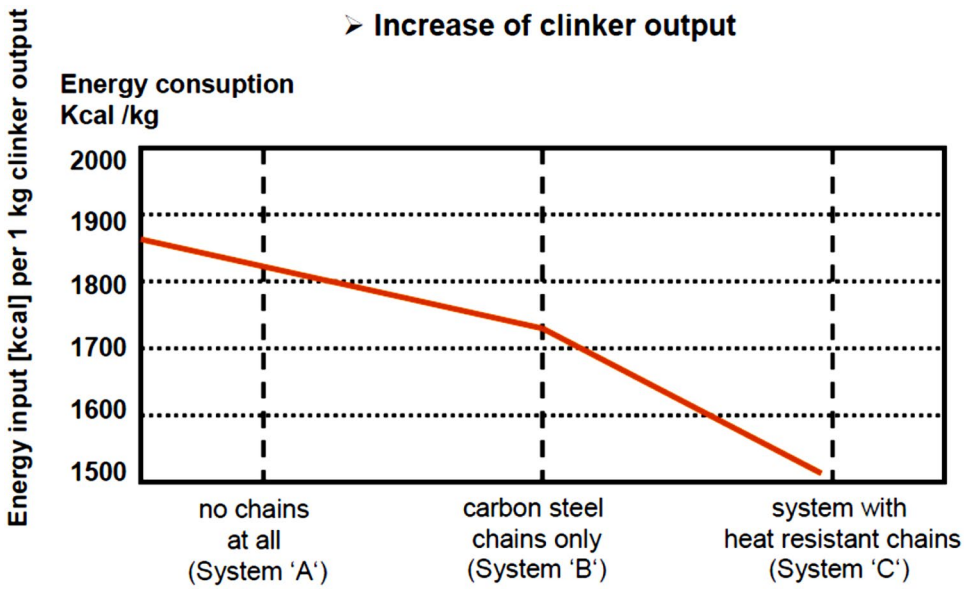

Fig. 3 The relationship between energy consumption with and without using chain curtains [2]

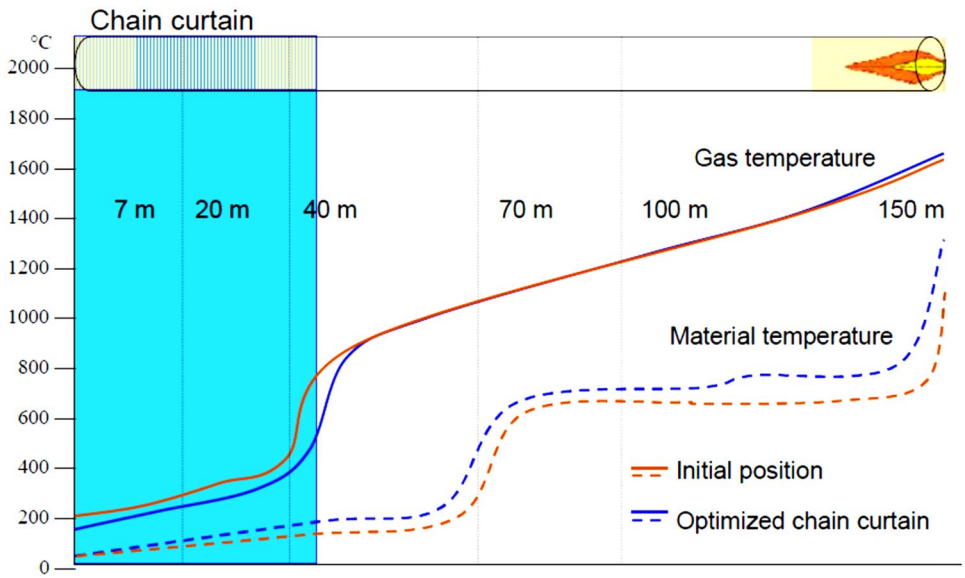

Fig. 4 The typical distribution of temperature of gas and material along the kiln length [2]

cement kiln continuous operation. Two types of steel grades are in service, DIN 1.4742 grade with ring dimension of (80 ϕ × 20 thick) usually located at the first four meters of the kiln chains curtain. The other cheaper steel grade is St37 with ring dimensions of (81 ϕ × 25 thick and 65 ϕ × 20 thick) depending on the location from the kiln flame. The chemical composition of the material under study is shown in Table 1 which includes 1.4742 (AISI F10) and St37 steel grades.

Chains Collection and Preparation

Ten rings have been collected from different locations starting from the first raw until 28.2 m from the curtain, and these rings have been experienced maximum operational temperature of 800 °C at the first raw for 30 days of continuous working. Two rings were taken from each location including the top and bottom ring in order to compare the chemical analysis and the change in dimensions. The same mentioned method of samples collection has been carried out after 180 days of continuous work inside the rotary cement kiln. In total, 11 rings were collected

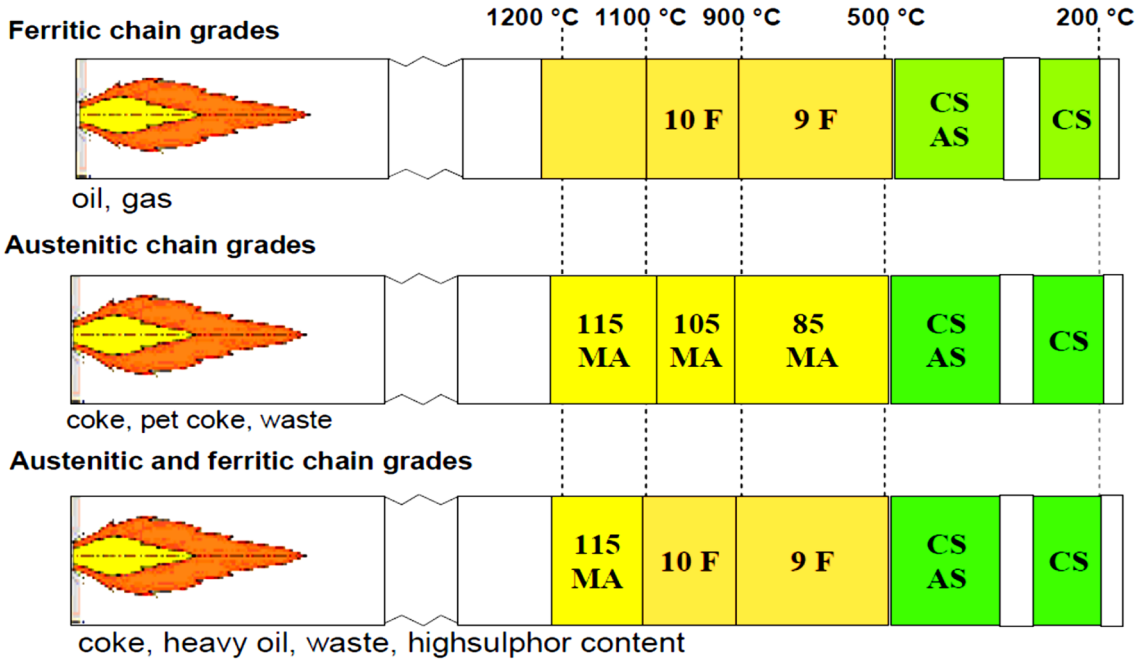

Fig. 5 The ideal suggested layout of chains designed by Heko Ketten company, Germany, which depends on the fuel type [2]. CS—carbo steel, AS—austenitic steel, 9F and 10F—ferritic steels, 115MA, 105MA, and 85MA—new developed austenitic manganese steels

including top and bottom rings, and the last ring at 28.2 m made of 1.4742 (AISI F10) steel grade has been replaced St37 grade on the purpose to study the effect of the distance from fire on the change of chain chemical composition and dimensions. The reductions in chain thickness and diameter have been measured accurately using digital vernier calliper. Each ring has been cut into two halves using electric saw in order to take a cross-sectional specimen (2 mm thick) for chemical analysis. (Specimens can be taken from any position on the chain as the whole chain was experienced a uniform thermo-chemical-mechanical effect.) For optical microscopy and SEM-EDS tests, cross-sectional specimens of 10 mm thick were taken from each steel ring. Grinding, polishing, and etching by 2% nital have been applied for microscopy purpose.

Chemical Analysis

Chemical analysis using inductively coupled plasma (ICP) has been carried out on each ring specimen in order to calculate the chemical weight (wt.%) for elements starting from C to Fe. Model JY48P ICP atomic emission spectrometer was used. Twenty-two elements of 1.4742 (AISI F10) steel grade and twenty-six elements for St37 steel grade have been analyzed. Specimens were acidified with 1% ultrapure hydrochloric acid and nitric acid in order to dissolve the metal. The salts have been dissolved with hydrochloric acid (7–8 N) and extracted three times with methyl isobutyl ketone (MIBK). More details about the ICP technique can be found in Yoshihide and Noritaka [8].

Optical Microscopy

Optical images of 1.4742 (AISI F10) including unused, used for 30 days and used for 180 days have been produced to highlight the possible change in the microstructure grain sizes. Images were obtained using (Lyceum microscope).

SEM Images and SEM-EDS Analysis

Energy-dispersive x-ray spectroscopy EDS-SEM was carried out on the polished and etched (2% nital) samples using FEI Nova Nano SEM in order to analyze the possible segregation of elements. The SEM produced high-quality and high-resolution images of microconstituents by employing secondary electron (SE) imaging mode with accelerated voltage 20 kV which gives high penetration. The working distance (WD) used was 5 mm but in some cases altered (decreased or increased) to enhance the contrast at high magnification. The main aim for this microstructural assessment is to generate important information regarding the elements segregation in steel.

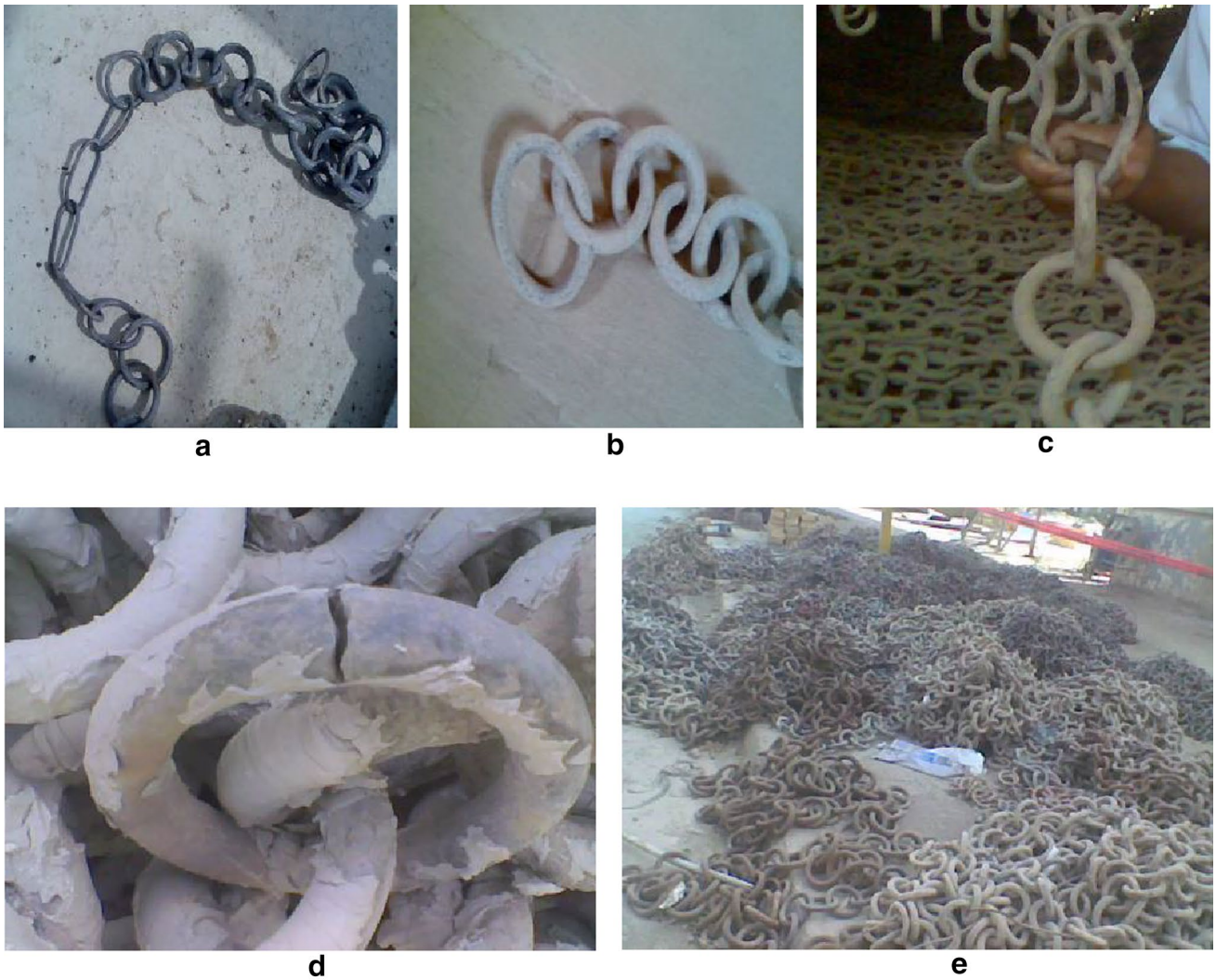

Fig. 6 Different types of chains failure, (**a**) reduction in thickness and deformation (St37 grade), (**b**) oval deformation in the first ring, 1.4742 (AISI F10). (**c**) Reduction in thickness, oval, and twisting deformation in the first ring 1.4742 (AISI F10). (**d**) Brittle cracking (DIN 1.4892 105MA) and (**e**) different types of failed chains dropped outside the cement kiln. Courtesy of *Kufa cement plant* (image no. CK-007-CK011)

Table 1 Chemical Composition of DIN 1.4742 (AISI F10) and St37 Steel Grades (wt.%)

	C%	Si%	Mn%	P%	S%	Cr%	Ni%	Mo%	Al%	Cu%	Co%
1.4742	0.12	1.2	1	0.04	0.015	19	0.6	0.12	1.2	0.2	0.018
St37	0.17	0.3	1.4	0.05	0.05	0.3	0.3	0.05	0.05	0.4	0.1
	Ti%	Nb%	V%	W%	Pb%	B%	Sn%	As%	Bi%	Ca%	Fe%
1.4742	0.01	0.01	0.048	0.01	0.003	0.001	0.011	0.0057	0.0015	0.0005	Balance
St37	0.03	0.03	0.03	0.1	0.05	0.0005	0.024	0.014	0.002	0.0003	Balance

Microhardness Measurement

Measuring the hardness can give a good estimation for the microstructure without examining the morphology. Hardness was measured using Vickers microhardness device (HV) by applying 300-gf load with a diamond indenter. The measurement was taken along the horizontal and vertical surfaces of the samples under study in order to increase the accuracy.

Results

Samples Collection and Preparation

Figures 7 and 8 show the collected samples after continuous work inside the rotary cement kiln for 30 and 180 days, respectively. The samples arranged according to the distance and deformation, and each sample has been cut into two halves in order to take a specimen for chemical analysis, optical, and SEM-EDS tests. The details of samples location, materials type, actual dimensions, and the original dimensions are listed in Tables 2 and 3 for 30 and 180 days of continuous work, respectively.

Optical and SEM-EDS of Unused 1.4742 Chain

Figure 9 is an optical image that shows the microstructure of unused 1.4742 chains, and the SEM-EDS of the elemental precipitates is shown in Figs. 10 and 11.

Optical, SEM-EDS, and Chemical Analysis of the Used Chains

Figure 12a and b shows optical and SEM images of 1.4742 steel (top ring) chain after using for 30 days inside the rotary cement kiln. Figures 13, 14, 15, and 16 show optical, SEM-EDS, and SEM images, respectively, of 1.4742 steel (top ring) chain after using for 180 days inside the rotary cement kiln. Figure 17 is an SEM-EDS mapping for the segregated elements. Table 4 shows the results of ICP chemical analysis of ring 1 to ring 21. Table 5 summarizes the loss of chromium and carbon due to segregation for all the samples under study, while Table 6 suggests alternative steel grades that may hold for longer time inside the rotary cement kiln.

Discussion

Chains Deformation and the Reduction in Thickness

Table 2 shows the change in ring dimensions after 30 days of serving inside *Kufa* rotary cement kiln. The top ring of 1.4742 grade at the first row (sample 1) has shown the maximum reduction in thickness (2 mm), while the bottom

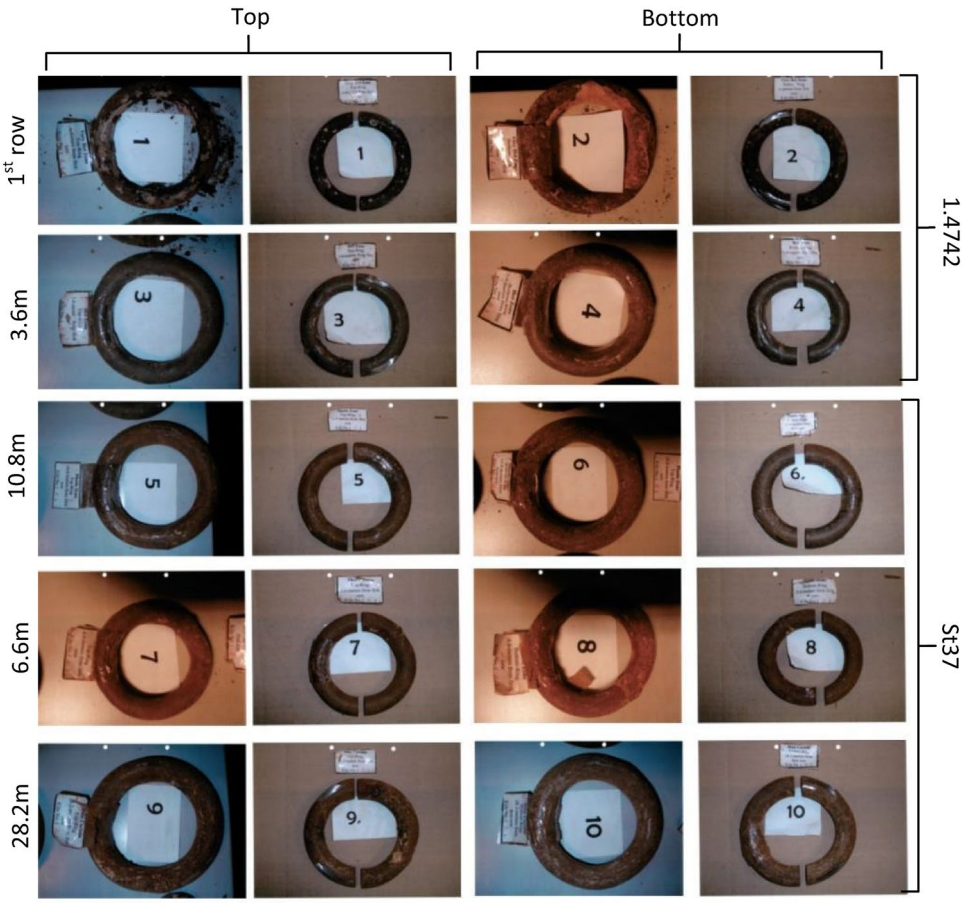

Fig. 7 Samples of chains taken from different distances from the fire of cement kiln after 30 days of continuous work, each sample has been cut into two halves, and cross-sectional specimens were taken from each half for chemical analysis and imaging test. The location of the samples has been assigned to the left of the image, whereas the steel grade was assigned to the right of the image

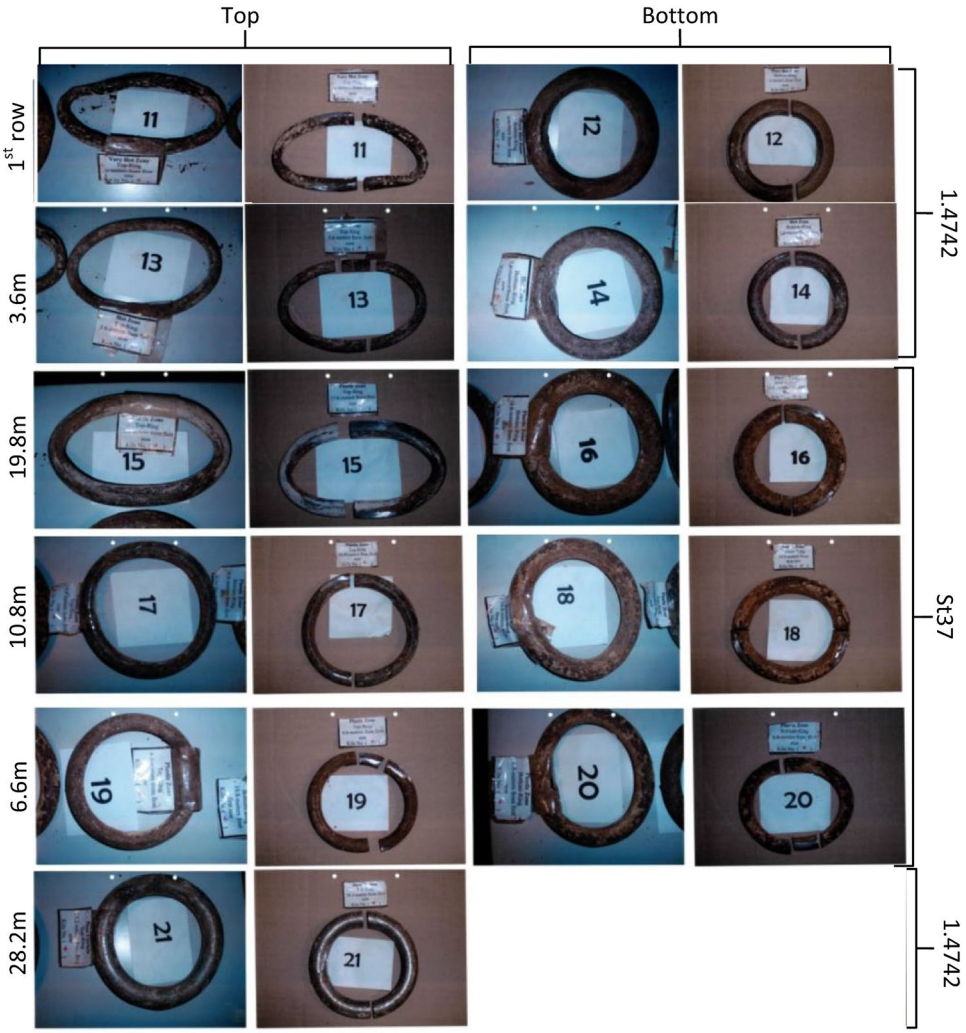

Fig. 8 Samples of chains taken from different distances from the fire of cement kiln after 180 days of continuous work, each sample has been cut into two halves, and cross-sectional specimens were taken from each half for chemical analysis and imaging test. The location of the samples has been assigned to the left of the image, whereas the steel grade was assigned to the right of the image

Table 2 The details of the deformation and the distance from the kiln flame for the top and bottom chains (30 days of continuous using)

Sample no.	Distance from the fire, m	Top/bottom	Actual dimensions mm		Original dimensions mm		Reduction in thickness, mm	Actual material
			Thickness	Diameter	Thickness	Diameter		
1	1st raw	Top	18	80	20	80	2	14.742
2	1st raw	Bottom	20	80	20	80	0	14.742
3	3.6 m	Top	20	80	20	80	0	14.742
4	3.6 m	Bottom	20	65	20	65	0	14.742
7	6.6 m	Top	14–19	65	20	65	6–1	St 37
8	6.6 m	Bottom	19	65	20	65	1	St 37
5	10.8 m	Top	24	80	25	81	1	St 37
6	10.8 m	Bottom	25	80	25	81	0	St 37
9	28.2 m	Top	24	80	25	81	1	St 37
10	28.2 m	Bottom	25	80	25	81	0	St 37

ring was not affected. The reduction in thickness of the top ring can be related to corrosion abrasion of the ring surface which resulted from the thermo-chemical-mechanical effects. The top ring carries all other 44 rings which weigh together 35.2 kg, add to that the effect of drag forces when the chains are in contact with the mud during kiln rotation. The abrasion between the surfaces of the top ring and the second ring in a corrosive environment during

Table 3 The details of the deformation and the distance from the kiln flame for the top and bottom chains (180 days of continuous using)

Sample no.	Distance from the fire, m	Top/bottom	Actual dimensions mm		Original dimensions mm		Reduction in thickness, mm	Actual material
			Thickness	Diameter	Thickness	Diameter		
11	1st raw	Top	13	50–120	20	80	7	1.4742
12	1st raw	Bottom	19	80	20	80	1	1.4742
13	3.6 m	Top	11	62–111	20	80	9	1.4742
14	3.6 m	Bottom	14	70	20	65	6	1.4742
19	6.6 m	Top	13	66–77	20	65	7	St 37
20	6.6 m	Bottom	13	74	20	65	7	St 37
17	10.8 m	Top	15	92	25	81	10	St 37
18	10.8 m	Bottom	19	80–90	25	81	6	St 37
15	19.8 m	Top	16	58–121	25	81	9	St 37
16	19.8 m	Bottom	21	81	25	81	4	St 37
21	28.2 m	Top	18	77	25	81	7	1.4742

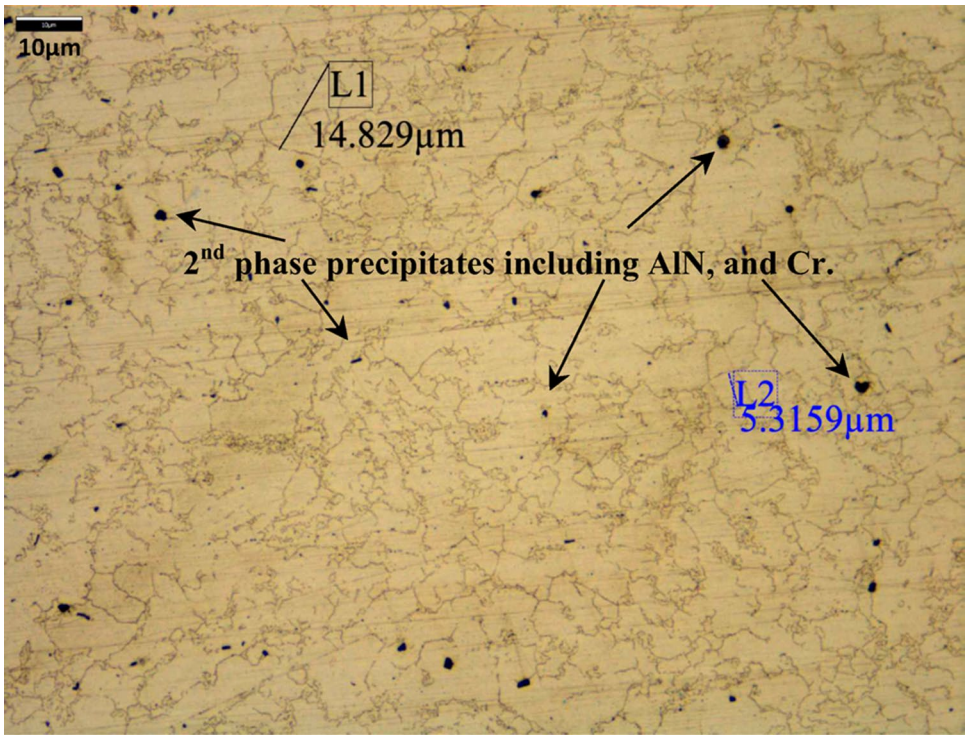

Fig. 9 Optical microscopy image of DIN 1.4742 (AISI F10), average grain size is 10 µm. The black spot is the second-phase precipitates including AlN and Cr

the kiln rotation can be the main reason of top ring thickness reduction. This was also clear in the top ring of St37 steel grade (sample 7) where the ring lost 1–6 mm from its original thickness. Top rings of sample 5 and sample 9 have experienced a reduction in thickness of 1 mm for the same mentioned thermo-chemical-mechanical effects. It is worth to highlight that rings with a distance closer to kiln fire (sample 1 and sample 7) have experienced more reduction in thickness compared to other rings. The original diameter of 1.4742 grade samples does not affect by creep after serving for 30 days as this grade includes high percentage of Cr, Ni, and other elements (see Table 1) which enabled the microstructure to resist the creep phenomenon. The differs in atoms size of the alloying elements exist in steel alloy can interrupts the arrangement order of the iron atoms in the lattice space and thus the creep by sliding mechanism will be difficult to occur [9]. Rings of St37 grade including samples 5, 6, 9, and 10 have shown a

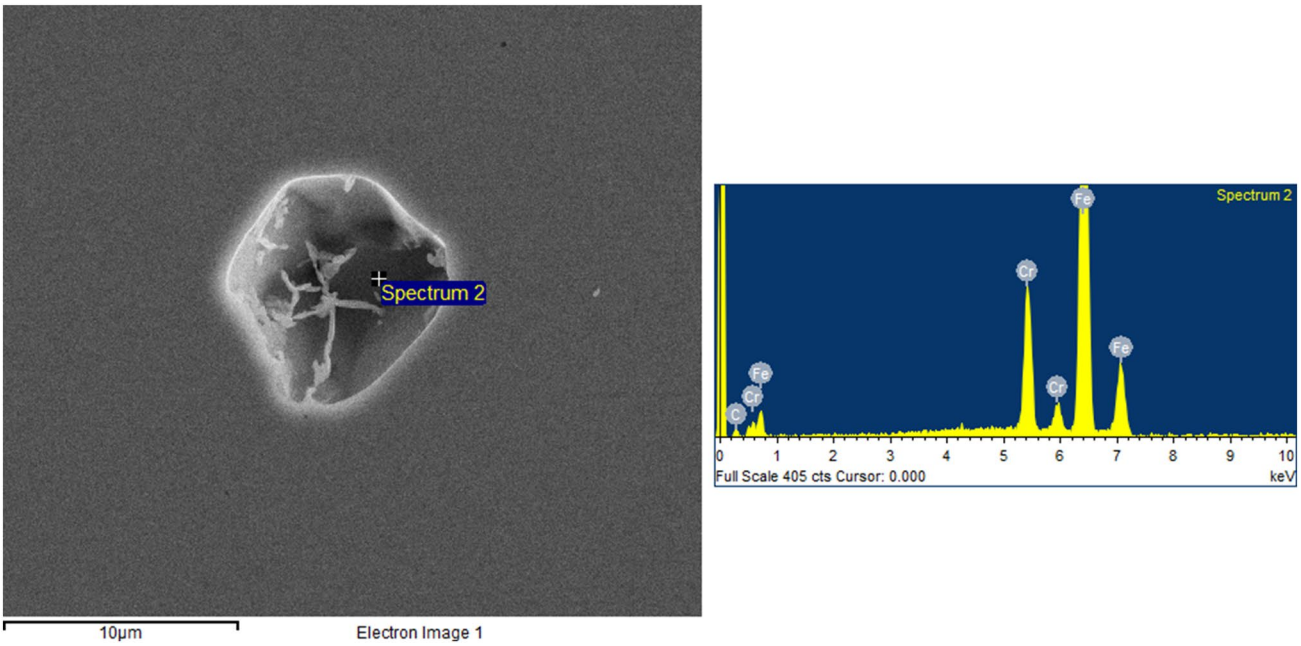

Fig. 10 SEM-EDS of unused chain 1.4742 (AISI F10) shows chromium in the microstructure

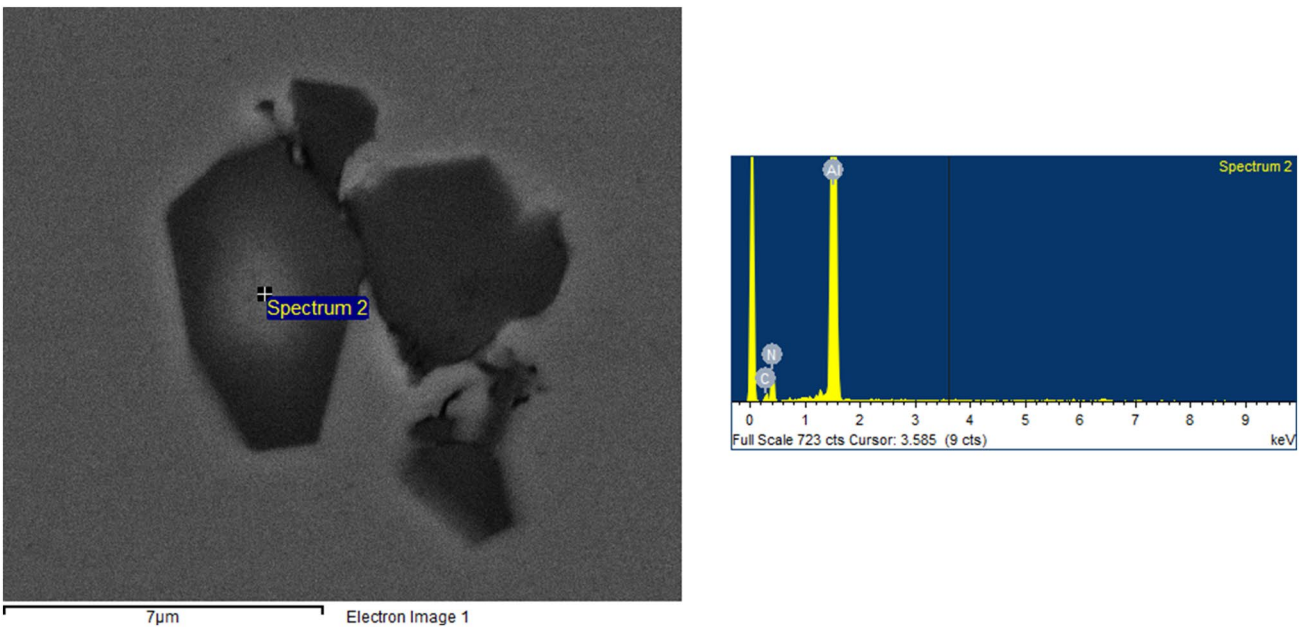

Fig. 11 SEM-EDS of unused chain 1.4742 (AISI F10) shows AlN in the microstructure

change in original diameter equal to 1 mm which resulted from creep behavior as less alloying elements exist in this steel grade (see Table 1). Creep will not be detailed in this work as it focuses mainly on elemental segregation; however, more details about creep can be found in Zauter et al. [10].

Table 3 shows the change in ring dimensions after 180 days of continuous working inside *Kufa* rotary cement kiln. Top rings have been recorded the maximum reduction in thickness; it also showed a significant deformation (oval shape) especially in the first rows (sample 11 and sample 13) as shown in Fig. 8 and Table 3. The oval shape of the top rings can be attributed to the uniform continuous

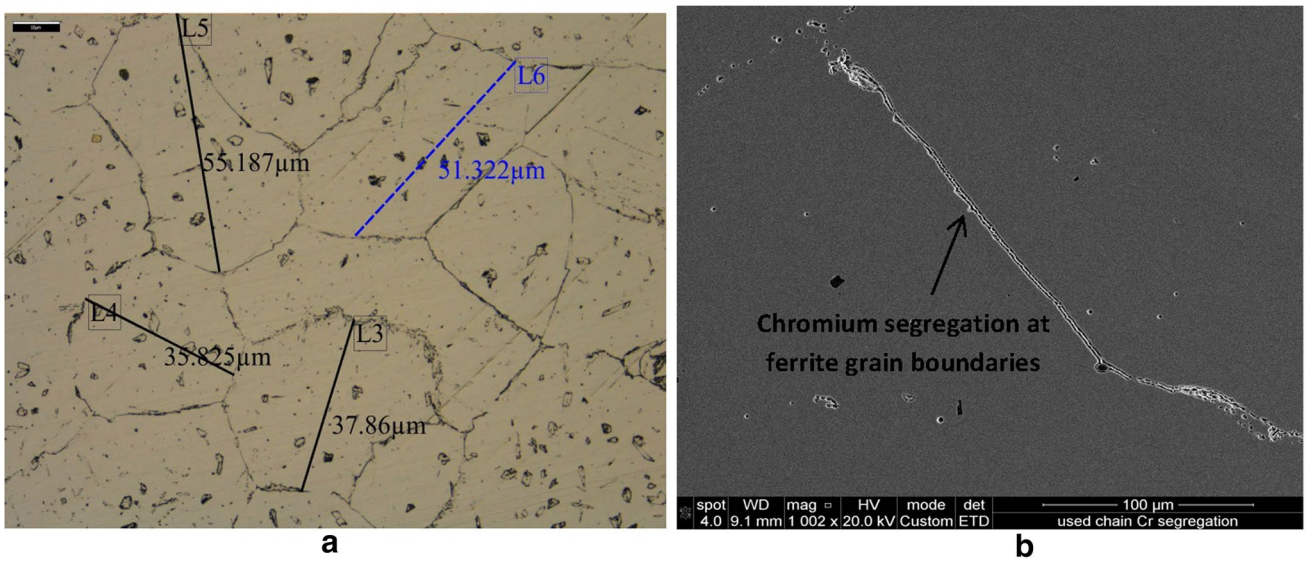

Fig. 12 Images of 30 days used chain DIN 1.4742 (AISI F10) first row, (**a**) optical microscopy, average grain size is 45 µm, and the dark second phase is chromium segregation. (**b**) SEM segregation of Cr at ferrite grain boundaries

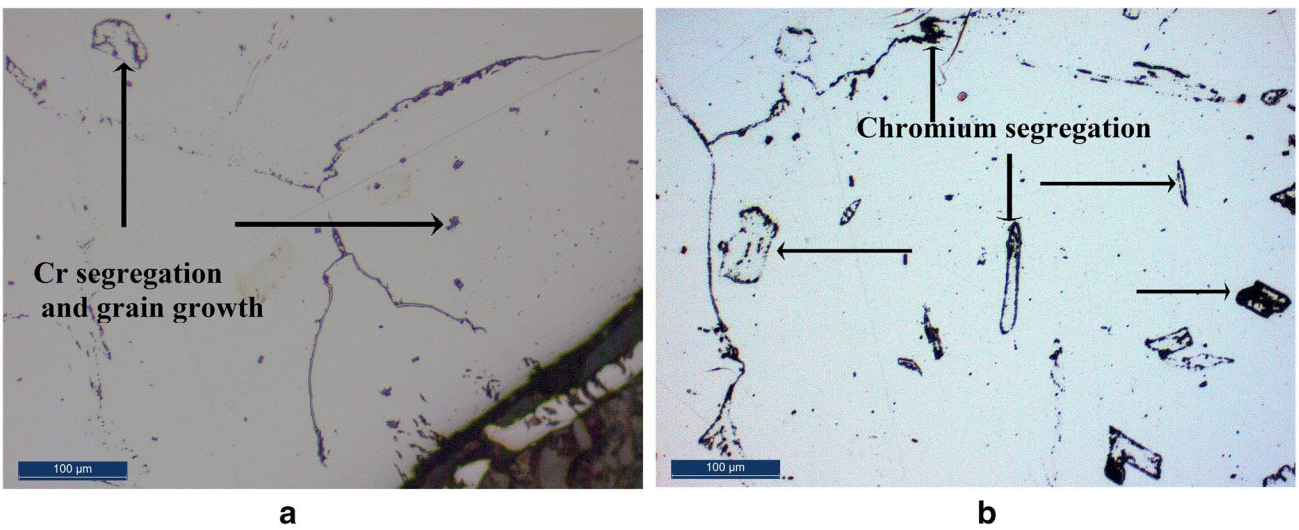

Fig. 13 Optical images of 180 days used chain DIN 1.4742 (AISI F10) first row, (**a**) chain edge, (**b**) chain middle, both images show grain growth and segregation of Cr within ferrite grain and also at ferrite grains boundaries, average grain size is 550 µm. The dark second phase is chromium segregation

reduction in thickness and also to the creep behavior under the effect of loading and heating. Creep behavior needs more investigation, and the current study concentrates on the Cr segregation as a main cause of chains failure. The reduction in chains thickness as shown in Table 3 was independent on the rings distance from fire which can be attributed to the long continuous working. Example of that is samples 13 and 17 which showed higher reduction in thickness compared to samples 11 and 19, despite the fact that the distance from fire was longer in the case of samples 13 and 17. This also can be noticed in sample 21 which showed the same reduction in thickness of sample 11 despite the high difference of the distance from fire.

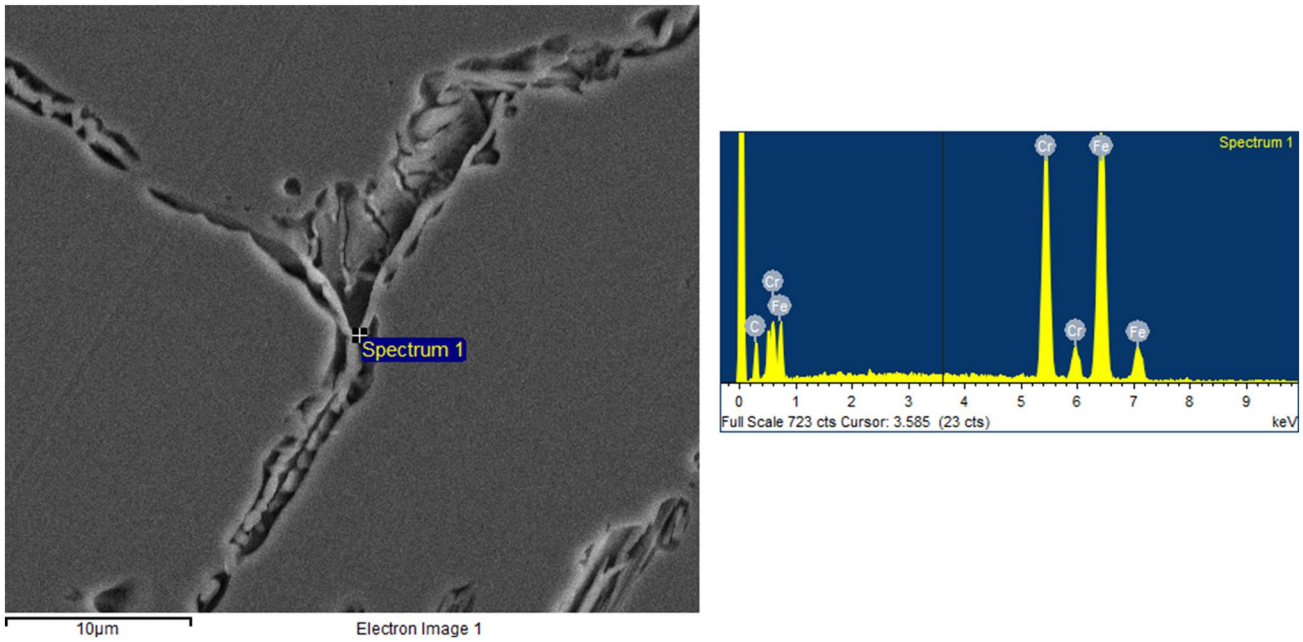

Fig. 14 SEM-EDS analysis shows Cr-C segregation at ferrite grain boundaries, used chain DIN 1.4742 (AISI F10) first row for 180 days

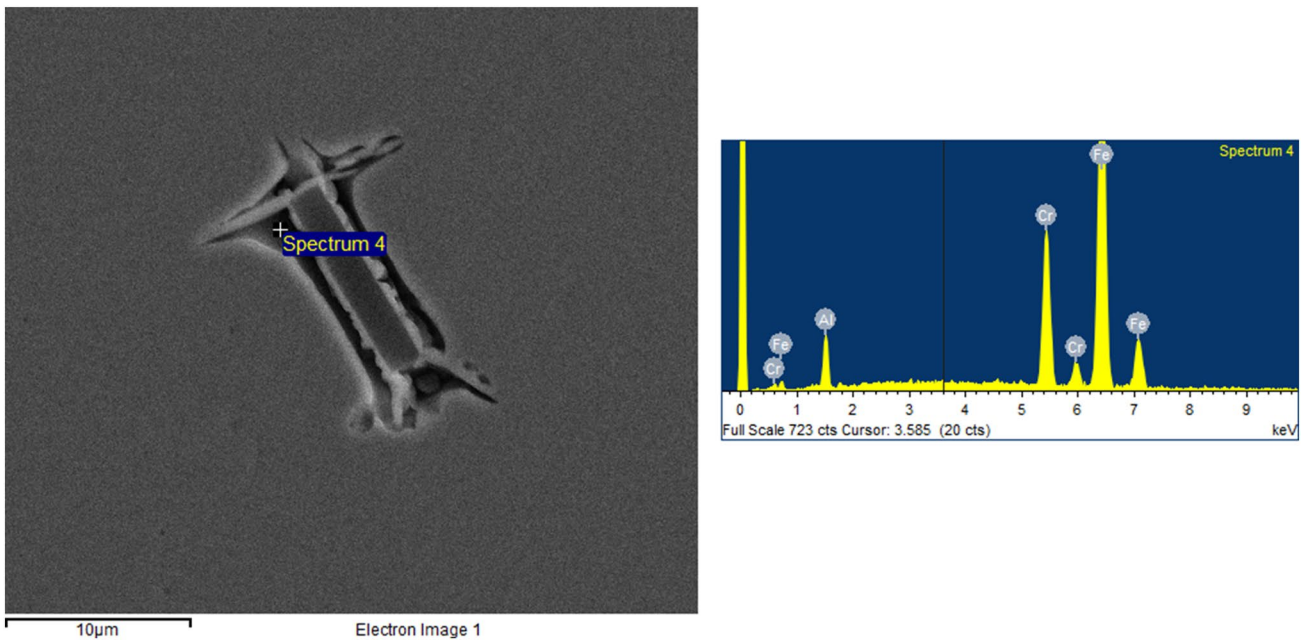

Fig. 15 SEM-EDS analysis shows Cr segregation around AlN, used chain DIN 1.4742 (AISI F10) first row for 180 days

Microstructure and Hardness Examination of Unused and Used Chains of 1.4742 Steel Grade

The microstructure of the unused 1.4742 steel grade as shown in Fig. 9 includes fine grains of ferrite with average grains size of 10 µm. The alloying elements under concern including Cr and Al are shown in the SEM-EDS in Figs. 10 and 11, respectively. Aluminum was found in a form of AlN which can control the ferrite grain size and thus increases the microstructure hardness [11]. Figure 12a and b shows the optical and SEM images of the chain microstructure after 30 days of continuous work inside the cement kiln. The microstructure has shown a grain growth with average grain size of 45 µm; this grain growth represents 4 times of

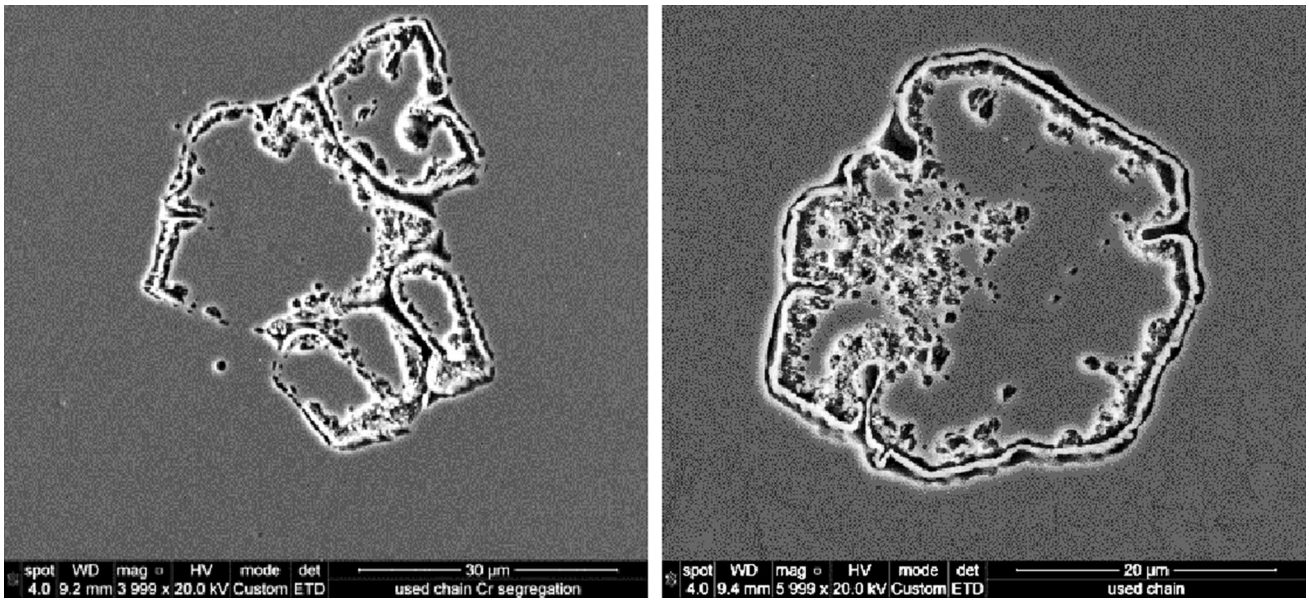

Fig. 16 SEM images show Cr segregation within ferrite grains, used chain DIN 1.4742 (AISI F10) first row for 180 days

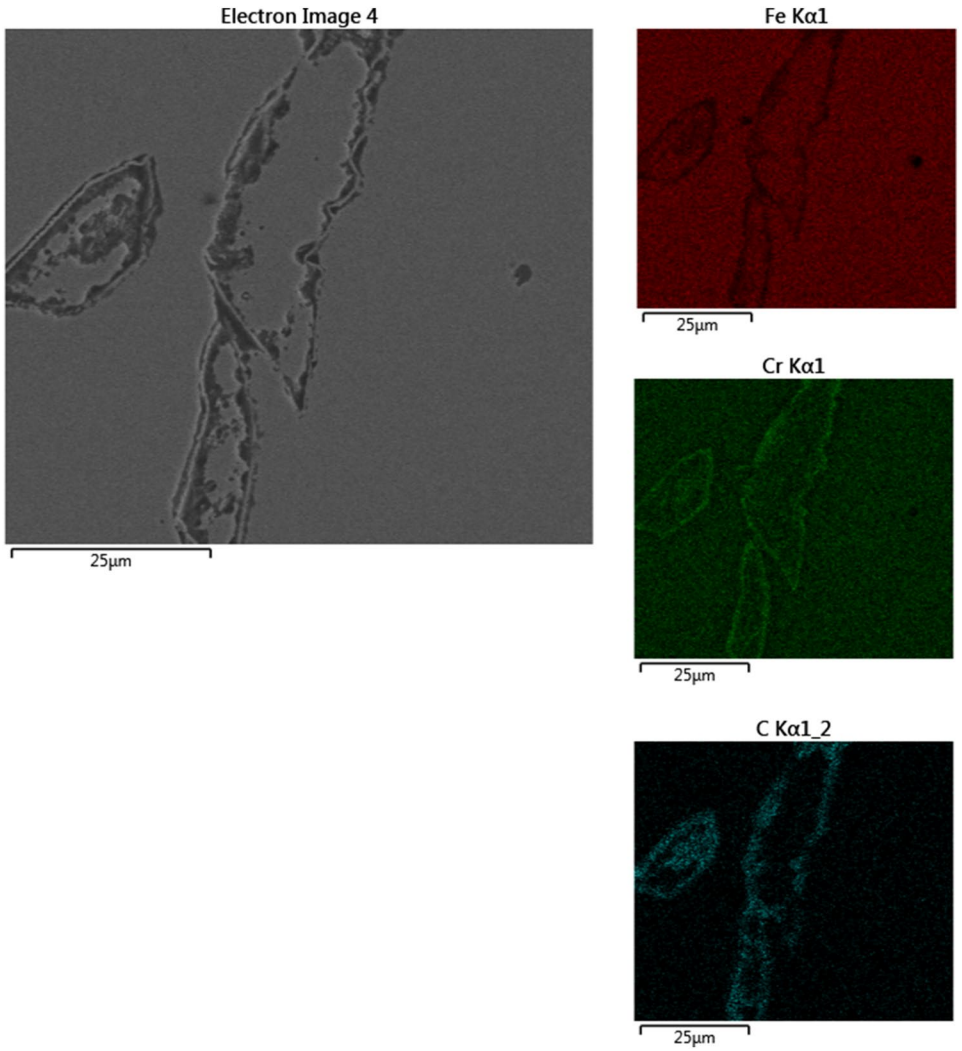

Fig. 17 Cr and C segregation within ferrite grains, SEM-EDS mapping technique, used DIN 1.4742 (AISI F10) first row for 180 days

Table 4 Chemical analysis (wt.%) for samples 1–21

	C%	Si%	Mn%	P%	S%	Cr%	Ni%	Mo%	Al%	Cu%	Co%
Sample 1	0.083	0.879	0.432	0.014	0.0036	17.30	0.498	0.156	1.03	0.093	0.022
Sample 2	0.075	0.840	0.399	0.017	0.0040	17.22	0.156	0.076	1.10	0.079	0.019
Sample 3	0.075	0.888	0.399	0.015	0.0040	17.28	0.156	0.085	1.10	0.078	0.019
Sample 4	0.092	0.870	0.448	0.015	0.0047	17.37	0.225	0.079	0.849	0.098	0.020
Sample 5	0.150	0.223	0.477	0.014	0.024	0.0062	0.0074	0.0039	0.001	0.0098	0.0045
Sample 6	0.169	0.215	0.579	0.019	0.027	0.020	0.0069	0.0074	0.001	0.04	0.0059
Sample 7	0.162	0.161	0.517	0.023	0.022	0.028	0.0095	0.0061	0.001	0.03	0.0061
Sample 8	0.168	0.186	0.502	0.0096	0.019	0.018	0.0080	0.0063	0.001	0.027	0.0048
Sample 9	0.146	0.075	0.380	0.021	0.019	0.016	0.008	0.0037	0.001	0.010	0.0039
Sample 10	0.141	0.144	0.481	0.019	0.018	0.015	0.0082	0.0057	0.001	0.052	0.0066
Sample 11	0.139	0.779	0.405	0.001	0.0021	16.47	0.038	0.025	2.52	0.047	0.0020
Sample 12	0.078	0.861	0.416	0.014	0.0035	17.43	0.160	0.085	0.883	0.055	0.0180
Sample 13	0.082	0.796	0.340	0.0016	0.0070	16.93	0.155	0.071	0.827	0.105	0.0180
Sample 14	0.080	0.863	0.407	0.013	0.0039	17.39	0.139	0.089	0.929	0.048	0.0190
Sample 15	0.160	0.159	0.490	0.018	0.024	0.033	0.022	0.0063	0.0032	0.040	0.0053
Sample 16	0.149	0.158	0.500	0.017	0.022	0.027	0.026	0.0060	0.0010	0.039	0.0072
Sample 17	0.180	0.176	0.499	0.0074	0.018	0.023	0.010	0.0057	0.0010	0.032	0.0050
Sample 18	0.146	0.195	0.557	0.012	0.027	0.018	0.0092	0.0061	0.0010	0.037	0.0062
Sample 19	0.17	0.181	0.518	0.012	0.019	0.030	0.021	0.0077	0.0011	0.043	0.0067
Sample 20	0.145	0.199	0.531	0.0069	0.013	0.0089	0.0088	0.0046	0.0015	0.012	0.0074
Sample 21	0.09	0.825	0.696	0.017	0.0047	18.30	0.532	0.117	0.908	0.109	0.018
	Ti%	Nb%	V%	W%	Pb%	B%	Sn%	As%	Bi%	Ca%	Fe%
Sample 1	0.0074	0.004	0.084	0.010	0.0030	0.0007	0.0088	0.0019	0.0015	0.0004	79.38
Sample 2	0.0094	0.004	0.103	0.010	0.0030	0.0007	0.0077	0.0015	0.0015	0.0001	79.88
Sample 3	0.0094	0.004	0.105	0.010	0.0030	0.0008	0.010	0.0015	0.0015	0.0003	79.77
Sample 4	0.0054	0.004	0.103	0.010	0.0030	0.0009	0.0099	0.0019	0.0015	0.0010	79.81
Sample 5	0.0010	0.003	0.001	0.010	0.0030	0.0005	0.0010	0.0018	0.0020	0.0003	99.07
Sample 6	0.0010	0.003	0.0038	0.010	0.0030	0.0005	0.018	0.0016	0.0020	0.0006	98.86
Sample 7	0.0010	0.003	0.0033	0.010	0.0030	0.0005	0.014	0.0098	0.0020	0.0003	99.01
Sample 8	0.0010	0.003	0.0013	0.010	0.0030	0.0005	0.012	0.0082	0.0020	0.0039	99.03
Sample 9	0.0010	0.003	0.0010	0.010	0.0030	0.0005	0.016	0.0083	0.0020	0.0010	99.28
Sample 10	0.0010	0.003	0.0065	0.010	0.0030	0.0005	0.024	0.0140	0.0020	0.0003	99.01
Sample 11	0.0070	0.009	0.073	0.010	0.0030	0.0005	0.0040	0.0015	0.0015	0.0076	78.62
Sample 12	0.0057	0.004	0.089	0.010	0.0030	0.0006	0.0085	0.0015	0.0015	0.0005	79.88
Sample 13	0.0083	0.004	0.089	0.010	0.0030	0.0006	0.0063	0.0015	0.0015	0.0034	80.56
Sample 14	0.0095	0.004	0.104	0.010	0.0030	0.0007	0.0097	0.0020	0.0015	0.0006	79.89
Sample 15	0.0010	0.003	0.0015	0.010	0.0030	0.0005	0.018	0.018	0.0020	0.0014	99.00
Sample 16	0.0010	0.003	0.0016	0.010	0.0030	0.0005	0.019	0.016	0.0020	0.0005	99.01
Sample 17	0.0010	0.003	0.0021	0.010	0.0030	0.0005	0.016	0.0079	0.0020	0.0004	99.02
Sample 18	0.0010	0.003	0.0021	0.010	0.0030	0.0005	0.018	0.014	0.0020	0.0004	98.95
Sample 19	0.0010	0.003	0.0015	0.010	0.0030	0.0005	0.013	0.012	0.0020	0.0009	98.96
Sample 20	0.0010	0.003	0.0010	0.010	0.0030	0.0005	0.017	0.0019	0.0020	0.0004	99.05
Sample 21	0.0091	0.0044	0.047	0.010	0.003	0.001	0.011	0.0057	0.0015	0.0004	78.30

the grain sizes of the unused chain. It is also shown that a segregation of chromium within the ferrite grains but more at the ferrite grain boundaries as shown in Fig. 12b has occurred. Figure 13 shows the higher grain growth of 1.4742 grade microstructure after 180 days of continuous work. The average grain size has reached 550 μm due to grains coalescence, whereas chromium segregation (the second phase with dark color) is clear within the ferrite grains and also at

Table 5 The difference in chemical composition (Cr and C) of DIN 1.4742 (AISI F10) and St37 steel grades (wt.%) after 180 days of continuous work

	Steel grade	Top/bottom	Working period, days	The loss in C%	The loss in Cr%
Sample 1	1.4742	Top	30	− 0.037	− 1.7
Sample 2	1.4742	Bottom	30	− 0.045	− 1.78
Sample 3	1.4742	Top	30	− 0.055	− 1.72
Sample 4	1.4742	Bottom	30	− 0.028	− 1.63
Sample 5	St37	Top	30	− 0.02	− 0.2938
Sample 6	St37	Bottom	30	− 0.01	− 0.28
Sample 7	St37	Top	30	− 0.08	− 0.272
Sample 8	St37	Bottom	30	− 0.02	− 0.282
Sample 9	St37	Top	30	− 0.024	− 0.284
Sample 10	St37	Bottom	30	− 0.029	− 0.285
Sample 11	1.4742	Top	180	+ 0.019	− 2.53
Sample 12	1.4742	Bottom	180	− 0.042	− 1.57
Sample 13	1.4742	Top	180	− 0.038	− 2.07
Sample 14	1.4742	Bottom	180	− 0.04	− 1.61
Sample 15	St37	Top	180	− 0.01	− 0.267
Sample 16	St37	Bottom	180	− 0.021	− 0.273
Sample 17	St37	Top	180	+ 0.02	− 0.277
Sample 18	St37	Bottom	180	− 0.024	− 0.282
Sample 19	St37	Top	180	+ 0.03	− 0.279
Sample 20	St37	Bottom	180	− 0.025	− 0.2911
Sample 21	1.4742	Top	180	− 0.03	− 0.5

Table 6 Proposal of steel grades according to the distance from the kiln flame

Distance from the fire	Actual material in use	Our proposal	Reason
1st raw	14.742	1.4892-115 MA	Austenitic manganese steel grade that can hold up to 1200 °C, the high amount of Mn increases protection of Ni and reduces Cr segregation [1, 2]
3.6 m	14.742	1.4892-105 MA	Austenitic manganese steel grade that can hold up to 1000 °C, the high amount of Mn increases protection of Ni and reduces Cr segregation [1, 2]
6.6 m	St 37	1.4724 (AISI 9F)	A ferritic steel grade that can hold up to 750 °C, the steel grade includes high amount of Cr, i.e., 13%, which can increase the resistance toward corrosion [1, 2]
10.8 m	St 37	1.4724 (AISI 9F)	A ferritic steel grade that can hold up to 750 °C, the steel grade includes high amount of Cr, i.e., 13% which can increase the resistance toward corrosion [1, 2]
19.8 m	St 37	C35 (AISI C1035) not hardened	Cheap ferrite/pearlite steel grade that can hold up to 500 °C, as the temperature at this location is no exceeding 400 °C
28.2 m	St 37	C35 not hardened	Cheap ferrite/pearlite steel grade that can hold up to 500 °C as the temperature at this location is no exceeding 350 °C

ferrite grain boundaries. Chromium segregation as revealed by SEM-EDS shown in Fig. 14 has taken a band-like shape. It also segregated around the AlN precipitates as shown in Fig. 15. Within the ferrite grains, chromium segregated in closed rings as shown in Fig. 16a and b. The band-like pattern segregation of Cr has reported previously in 434 stainless steel as a result of experiencing hot rolling [7]. The Cr segregation has been mentioned in the literature review and interpreted as micro-galvanic corrosion that cause a Cr segregation, the steel grain act as anode whereas the grain boundary act as cathode [4].

The microhardness test of the unused chain has shown an average value of 180HV Kgf/mm^2, whereas the used chain (180 days of continuous working) has shown localized microhardness. An average value of 166HV Kgf/mm^2 in the microstructure away from the chromium segregation regions

has been measured. The decrease in the microhardness of the used chain can be attributed to the grain growth which in turn has reduced the grain boundaries density, and thus, wear resistance is expected to decrease. The regions which showed Cr segregation have shown higher microhardness value of 200HV Kgf/mm^2 as a result of forming mainly chromium carbides as revealed by SEM-EDS mapping in Fig. 17.

Chemical Analysis

Although the chemical analysis has been carried out for many alloying elements, the focus will be on the chromium and carbon as these elements showed a significant segregation in the used chain microstructure as discussed in the previous section. Generally speaking, most of the alloying elements have shown a decrease in the chemical percentage (wt.%) as a result of segregation. The decrease in wt.% of chromium due to segregation in 1.4742 grade has ranged from 2.5 at the top chain to 1.5 at bottom chain in the first row as reported in Table 5 samples 11 and 12, respectively. The average loss of carbon alloying element in 1.4742 steel grade after 180 days of continuous work was about 0.04% as shown in Table 5. St37 steel grade showed a significant loss of Cr in the microstructure reached to 0.28% compare to 0.3% the total percentage exist in the microstructure. The average loss of carbon after 180 days of continuous work was about 0.025. Table 6 suggests a new steel grades to be used in *Kufa* rotary cement kilns according to the result of this study and depending on the location from the fire. Austenitic manganese steel grades were suggested at the first row until 5 m from the fire as these grades can hold at very high temperatures. The higher percentage of Mn that exists in this new steel grade can increase the protection of Ni and is expected to reduce Cr segregation [1, 2].

Conclusion

In conclusion, the kiln chain failure has been investigated by carrying out many experiments including chemical analysis, optical images, SEM-EDS, and microhardness. The loss of alloying elements especially chromium due to the segregation has been detected as the main reason for the kiln chain failure. Chromium losing from the chains microstructure has reduced the corrosion resistance. The grains growth during service period has also increased the possibility of peeling the material away from the chain surface which in turn caused in reduction of thickness and also chains deformation. Using higher steel grades in the first row until 4–5 m from the cement kiln fire can increase chains longevity and reduce the chains failure. Such steel grades which include higher amount of Mn are 1.4892-115 MA and 1.4892-105 MA.

Future Work

- To examine the duty of the suggested chains and to compare with the current chains.
- To carry out thermo-mechanical tests on the chains including creep and hot bending.

Acknowledgments The author would like to thank the Ministry of Higher Education/the Research and Development Department, Iraq, and *Kufa* cement plant for funding this pioneer research project. The authors also would like to thank Mr. Khudier Abbas for his help in collecting data and samples.

References

1. Advanced Material Handling LTD., Kiln Chains and Accessories. http://www.advancedmaterial.ca/wp-content/uploads/2016/02/kiln_chain_brochure.pdf. Accessed May 2017
2. Heko Ketten GmbH, Kiln Chains and Accessories for Wet and Long-Dry Rotary Kilns. http://www.heko.com/index.php?id=306. Accessed May 2017
3. D. Stavrev, Ts. Dikova, Corrosion of Cr–Mn–Ni heat-resistant steel under thermocyclic and mechanical impact in furnace media. *Scientific Proceedings (VIII) International Congress "Machines, Technologies, Materials"* (2011), pp. 5–8
4. S.A. Park, W.S. Ji, J.G. Kim, Effect of chromium on the corrosion behaviour of low-alloy steels containing copper in FGD environment. Int. J. Electrochem. Sci. **8**, 7498–7509 (2013)
5. L.V. Saraf, A.S. Lea, C.M. Wang, A. Dohnalkova, B.W. Arey, Chromium segregation at the grain boundaries in Ni–Fe–Cr alloy. Microsc. Microanal. **16**(2), 690–691 (2010)
6. M.S. Laws, P.J. Goodhew, Grain boundary structure and chromium segregation in a 316 stainless steel. Acta Metall. Mater. **39**(7), 1525–1533 (1991)
7. J.D. Defilippi, H.-C. Chao, Effect of chromium and molybdenum segregation on the ridging behaviour of 434 stainless steel. Metallurgical Transactions **2**, 3209 (1971)
8. E. Yoshihide, S. Noritaka, Influence of background on iron and steel analysis by inductively coupled plasma atomic emission spectrometry. Transactions ISIJ **23**, 789–795 (1983)
9. P.J. Cunat, Alloying Elements in Stainless Steel and Other Chromium-Containing Alloys (2004). Published in cooperation with the International Chromium Development Association, The publication is available in print from ICDA, 45 Rue de Lisbonne, F-75008 Paris, © Euro Inox 2004. www.euroinox.org
10. R. Zauter, E. Petry, H.J. Christ, H. Mughrabi, High temperature creep behaviour and microstructure development of AISI 304L stainless steel. Mater. Sci. Eng., A **124**, 125–132 (1990)
11. F.G. Wilson, T. Gladman, Aluminum nitride in steel. Int. Mater. Rev. **33**(1), 221–286 (1988). http://www.tandfonline.com/doi/abs/10.1179/imr.1988.33.1.221